Contents lists available at ScienceDirect

Applied Energy

journal homepage: www.elsevier.com/locate/apenergy

Hull geometry optimisation of wave energy converters: On the choice of the objective functions and the optimisation formulation

Anna Garcia-Teruel [a,*], Bryony DuPont [b], David I.M. Forehand [a]

[a] Institute for Energy Systems, School of Engineering, The University of Edinburgh, Edinburgh, EH9 3BF, United Kingdom
[b] School of Mechanical, Industrial, and Manufacturing Engineering, Oregon State University, Corvallis, OR, 97331, USA

ARTICLE INFO

Keywords:
Wave energy converter
Hull
Geometry
Single-objective optimisation
Multi-objective optimisation
Metrics

ABSTRACT

Wave Energy Converters (WECs) with optimised geometries and control systems have been developed in recent years to advance marine energy technologies towards commercialisation. In particular, a number of WEC hull geometry optimisation studies have been performed, due to the high cost reduction potential associated with the device structure. However, no standard and consistent method has been established for this purpose. For example, different optimisation formulations (single-objective and multi-objective), have been used, applying different optimisation algorithms. Additionally, a range of objective functions have been employed, where power maximisation has been represented through a variety of metrics, and cost minimisation expressed with diverse cost proxies. The goal of this study is to address the challenge of finding a suitable optimisation problem formulation with single-objective or multi-objective implementations, and the respective objective functions, that support the exploration of shapes that reduce the levelised cost of energy. Results show that submerged surface area cost proxies are more suitable for this purpose than volume-based cost proxies. Results from a multi-objective optimisation formulation can provide a good understanding of the solution space, whereas results from single-objective studies can be used for seeding these multi-objective optimisation approaches.

1. Introduction

A number of Wave Energy Converters (WECs) have been developed in recent decades aiming at producing improved device designs capable of high annual energy production at low costs. Different metrics have been used to compare these devices depending on the purpose of the study. The Levelised Cost of Energy (LCoE) is used in the energy generation industry as a metric that enables comparison between different technologies, based on their generation costs. It is also used within the wave energy sector to compare different devices. The LCoE describes the ratio of Capital (CapEx) and Operational (OpEx) Expenditures to the Annual Energy Production (AEP), discounted to their Present Values (PV), through a discount rate. This is used widely for energy system analysis [1], and for the comparison of more developed technologies, such as photovoltaic [2] or power-to-gas [3] systems. However, in the case of emerging technologies such as wave energy, it is difficult to use this metric at early design stages, given the lack of available information on costs. Simultaneously, the use of design optimisation to generate novel and improved WEC designs without going through expensive build and test iterations is key to advance these technologies.

For this reason, WEC geometry optimisation studies have been performed for different types of devices, such as single-body [4] and, two-body point-absorbers [5], terminators [6], attenuators [7], and oscillating water columns [8]. A review of previous WEC geometry optimisation and comparison studies was provided in [9]. In general terms, most studies were based on simple geometry definitions, such as cylindrical-type shapes or spheres, or were performed for specific device designs. Some more generic approaches in terms of geometry definition were applied by McCabe et al. [4] based on a B-spline surface representation of the hull, or Abdelkhalik et al. [10] based on the use of polynomial and Bezier curves for the representation of an axisymmetric hull shape. Most of the studies aimed at maximising overall power production and minimising costs, using single-objective formulations [4] or multi-objective formulations [5] to represent these competing objectives. A number of proxies were used to represent these objectives. However, design optimisation approaches rely on the use of suitable metrics for comparison and selection of potential solutions. For this reason, a number of methods for quantifying the trade-off between power generation and costs of different WEC designs have been developed with the goal of allowing device comparison.

From a power performance perspective, different metrics were applied to eight different types of WECs in [11]. Additionally, different Technology Readiness Levels (TRLs) have been identified at which

* Corresponding author.
E-mail address: a.garcia-teruel@ed.ac.uk (A. Garcia-Teruel).

https://doi.org/10.1016/j.apenergy.2021.117153
Received 23 December 2020; Received in revised form 10 April 2021; Accepted 23 May 2021

Nomenclature

f	Objective function (NA)
g	Equality constraint (NA)
h	Inequality constraint (NA)
H_{m0}	Significant wave height (m)
HV	Hypervolume (NA)
MaxGen	Maximum number of iterations defined for an optimisation (NA)
N_{Ind}	Number of individuals in genetic algorithm (NA)
N_{Parents}	Number of parents in genetic algorithm (NA)
$\bar{P}$	Mean annual produced power (W)
P_{pm}	Power per metre crest length (W/m)
$P_{PTO,MAX}$	PTO rating (MW)
R	B-spline surface function (NA)
S	Submerged surface area (m^2)
S_I	Submerged surface area calculated with Method I (NA)
T_e	Energy period (s)
V	Submerged volume (m^3)
v_n	Vertex (NA)
$\mathbf{x}$	Vector of decision variables (NA)
Δ	Solution space (NA)
η_c	Distribution index for crossover (%)
η_m	Distribution index for mutation (%)
λ	Wavelength (m)
Ω	Search space (NA)
ξ	Stroke (m)
AEP	Annual Energy Production (MWh)
CW	Capture Width (m)
CWR	Capture Width Ratio (%)
DoF	Degree of Freedom (NA)
GA	Genetic Algorithm (NA)
NSGA-II	Non-Dominated Sampling Genetic Algorithm (NA)
PM	Polynomial Mutation (NA)
PSO	Particle Swarm Optimisation (NA)
PTO	Power Take-Off (NA)
PV	Present Value (NA)
RAO	Response Amplitude Operator (–)
SBX	Simulated Binary Crossover (NA)
TPL	Technology Performance Level (NA)
TRL	Technology Readiness Level (NA)
WEC	Wave Energy Converter (NA)

different Technology Performance Levels (TPLs) can be expected [12]. Based on the review of a range of device design optimisation and comparison studies, the following was concluded in [9]. Overall, the use of mean annual power [4] is preferred, rather than Capture Width (CW) [13], Capture Width Ratio (CWR) [14], oscillation Response Amplitude Operator (RAO) [15,16] or velocity [17]. This is because: (1) The behaviour of the device is highly dependent on the resource and evaluating a device at a single wave height and period is not representative of its behaviour in a real sea. This results from the fact that, optimisation procedures using these approaches tend to converge on devices with a natural period equivalent to the studied wave period (e.g. [16]). (2) The device performance will vary depending on its power absorption capabilities. This cannot be taken into account when using RAO or velocity as a proxy for power performance. Even if an optimal control is used as in [4], rather than a more realistic control as suggested in [18], this allows the application of an upper limit on the AEP. (3) Certain measures of the device, such as the submerged volume, can be constrained to avoid the optimisation converging towards very big or very small devices, depending on the objective function. In this way, the use of device-dependent measures in the objective function, such as the characteristic length, can be avoided.

From a techno-economic perspective, metric comparison studies were performed by de Andrés et al. [19] and methods for economic assessment of WECs were reviewed by Astariz and Iglesias [20]. Yu et al. [21] have proposed a whole system economic model, however, only a few examples of models aiming at a whole system economic evaluation exist, such as that implemented by Teillant et al. [22]. In WEC geometry optimisation studies, device size has been commonly considered as a cost proxy, represented through device mass [10], volume [5,23], surface area [5,23], or characteristic length [24]. A preliminary study comparing the use of different objective functions in WEC hull geometry optimisation was presented by Garcia-Teruel et al. [23], where it was found that submerged surface area was a better representative for costs than submerged volume when using an adaptable geometry definition, such as based on a B-spline surface representation. However, when using simple shapes (e.g. cylindrical-type shapes) little difference was found in the optimisation results when applying volume versus surface-area-based cost proxies by Blanco et al. [5]. Mass and submerged volume can be considered equivalent in this context, given that the displaced water mass can be represented through the submerged volume and the density of water. The use of a characteristic width or length, which has different physical implications for different types of WECs, is not considered a suitable metric for use in a generic method for device comparison. That is, for example, for a terminator type surging device the characteristic width may be defined as the width of the device perpendicular to the predominant wave direction. However, if the device is floating or bottom-fixed its overall volume and surface area may vary significantly despite the characteristic width being the same which would result in an unfair comparison. Additionally, if looking at other types of devices such as attenuators, the characteristic length will likely be defined as the length of the device parallel to the wave direction rather than its width, so that it will be difficult to compare the CWR of different types of devices.

A lack of an established methodology for WEC hull geometry optimisation, and particularly a lack of consensus on the most suitable metric used in the objective function are identified. The present study addresses this gap by investigating the suitability of a range of objective functions for WEC hull geometry optimisation. This focuses on enabling a fair device comparison and the generation of shapes with properties that result in an increased AEP and reduced costs. Additionally, single and multi-objective optimisation formulations have different requirements for the objective functions. For this reason, both problem implementations when using different objective functions are compared. Establishing the most suitable methods for WEC design and comparison supports technology developers to generate improved preliminary device designs and serves funding bodies to evaluate different technologies.

The method used for the present study is summarised in Section 2. The cases using different objective functions and optimisation algorithm formulations are introduced in Section 3. The results obtained with different objective functions are then compared in Section 4.1. The multi-objective implementation results are shown in Section 4.2, where the most suitable implementation is identified, and the results are compared to the single-objective optimisation results. Finally, the main conclusions and method recommendations drawn from these studies are presented in Section 5.

2. Methodology

The key elements of a WEC hull geometry optimisation process were identified to be the geometry definition, the objective function and the optimisation procedure in [9], and are shown in Fig. 1. In a WEC geometry optimisation process, the geometry is defined through a number of design variables, the optimal values of which are searched in the optimisation process, so that an objective function is minimised or maximised. In a single-objective optimisation formulation a single objective function is used, whereas in a multi-objective optimisation formulation a number of objective functions are applied and the trade-off in their minimisation or maximisation is pursued.

The suitability of the key elements: (1) geometry definition and (2) optimisation algorithms used for a single-objective problem formulation were discussed in detail in [26]. In that study, it was found that using an adaptable geometry definition capable of generating diverse shapes, such as the approach proposed in [4], instead of simple shapes, such as a hemisphere, a vertical cylinder or a barge, could result in up to 224% higher objective function values. Preferred meta-heuristic optimisation algorithm implementations were also obtained for different problems considering single rigid-body floating devices oscillating in one or multiple Degrees-of-Freedom (DoFs) and with different objective functions. This led to an improvement in objective function values of up to 11% while reducing the computational time by up to 50% when compared to applying the method described by McCabe in [4]. Therefore in [26], the focus was on finding the most suitable approaches for defining the geometry and choosing the optimisation algorithm for a single-objective optimisation problem.

The focus of the present study is to investigate the suitability of the other key elements, which are the choice of the objective functions and their effect on optimal geometry, as well as, the suitability of the optimisation formulation. The investigated elements are framed in Fig. 1 with a dashed line. As such, the overall goal is to identify the most suitable WEC hull geometry optimisation approach. As in the previous study [26], this is done based on a rigid single-body floating device (e.g. point-absorber, terminator, or oscillating wave surge converter), however, the findings from these studies are expected to be applicable to a wider range of WECs with rigid hull structures. A detailed discussion of the implementation of the geometry definition and the hydrodynamic model, as well as the single-objective problem formulation is provided in [26], however, a brief overview of the main approaches and assumptions used for each of the key elements is introduced in the following for context. The considered case studies in terms of the different objective functions and the multi-objective optimisation formulation are presented in detail in Section 3.

2.1. Optimisation procedure

First, the general formulation of single-objective and multi-objective problems is introduced to establish the terminology that will be used in the subsequent sections and sub-sections to define each of the elements of the optimisation process.

Single-objective formulation

A single-objective optimisation problem is defined as a problem in which the optimal values for a number of decision variables x_i are searched so that an objective function $f(\mathbf{x})$ is minimised or maximised. The search space Ω, i.e. the full range of possible decision variable values, is constrained through bounds and non-linear constraints defining restrictions between certain variable combinations. The solution space Δ i.e. the space of feasible solutions for the studied objective function, can be constrained by various equality g_j and inequality h_k constraints. This is represented mathematically below in the standard form [27].

$$\begin{aligned} &\min f(\mathbf{x}) \\ &\text{objective function:} && f(\mathbf{x}), \quad \text{for} \quad f \in \Delta \\ &\text{decision variable:} && \mathbf{x} = \{x_1, \dots, x_m\} \in \Omega \\ &\text{equality constraint:} && g_j(\mathbf{x}) = 0 \quad \text{for} \quad j = 1, \dots, n \\ &\text{inequality constraint:} && h_k(\mathbf{x}) \leq 0 \quad \text{for} \quad k = 1, \dots, o \end{aligned} \tag{1}$$

Here f represents the objective function and $\mathbf{x}$ the vector of optimisation variables. The optimisation variables are the design variables that define the WEC hull shape. For the single-objective optimisation, a detailed study for the selection of the optimisation algorithms and their implementation was presented in [26]. Meta-heuristic optimisation algorithms (both Genetic Algorithms (GAs) and Particle Swarm Optimisation (PSO) algorithms) were applied and a total of 14 different implementations were compared. The shapes resulting in the highest objective function values in this previous study are used here to discuss the suitability of the objective function. It should be noted that although the shapes resulted from the same runs discussed in the previous study, the shapes themselves and the suitability of the objective functions were not discussed there.

Multi-objective optimisation

In Multi-objective Optimisation Problems (MOPs) optimal solutions for a problem with various conflicting objectives ($\mathbf{f}(\mathbf{x}) = \{f_1, f_2, \dots, f_n\}$) are searched. As opposed to the single-objective optimisation problem, more than one solution will be optimal depending on the relevance of each objective function. This can be written mathematically in the standard form [27].

$$\begin{aligned} &\min \mathbf{f}(\mathbf{x}) \\ &\text{objective functions:} && \mathbf{f}(\mathbf{x}) = \{f_1, f_2, \dots, f_n\} \\ &\text{decision variable:} && \mathbf{x} = \{x_1, \dots, x_m\} \in \Omega \\ &\text{equality constraint:} && g_j(\mathbf{x}) = 0 \quad \text{for} \quad j = 1, \dots, n \\ &\text{inequality constraint:} && h_k(\mathbf{x}) \leq 0 \quad \text{for} \quad k = 1, \dots, o \end{aligned} \tag{2}$$

Analogously to single-objective optimisation problems, the optimal values for a number of decision variables x_i are searched. The solution space Δ_l i.e. the space of feasible solutions for each objective function f_l, can be constrained by various equality g_j and inequality h_k constraints. To clarify how different solutions are compared here versus for single-objective implementations, the concept of Pareto dominance ($x \prec y$) is introduced. One solution is said to dominate another one, when it performs better in all, or is equally good but better in at least one, of the objective functions (Eq. (3))

$$\forall i \in 1, \dots, n : f_i(\mathbf{x}) \leq f_i(\mathbf{y}) \wedge \exists i \in 1, \dots, n : f_i(\mathbf{x}) < f_i(\mathbf{y}) \tag{3}$$

In Fig. 2 (a) possible solutions of a bi-objective optimisation problem are represented in the objective space, where the objectives are minimised. Solutions a to d are non-dominated solutions and hence have no other solutions within their dominance cones marked in blue. Solution e is dominated by solution b, and solution g represents a solution weakly dominated by solution e and strictly dominated by solutions b, c and f.

A solution not dominated by any other in the objective space is called Pareto optimal. The Pareto front represents the corresponding objective functions' values of a Pareto optimal set. The implementation and choice of multi-objective optimisation algorithms is based mainly on three conflicting goals [29].

1. **Proximity to true Pareto front**
   The estimated Pareto front should be as close as possible to the true Pareto front.[1]

[1] The true Pareto front is the Pareto front representing the objective function values of all optimal solutions. Pareto fronts found with the help of meta-heuristic methods will approximate the true Pareto front, but the optimality of the obtained solutions cannot be proven.

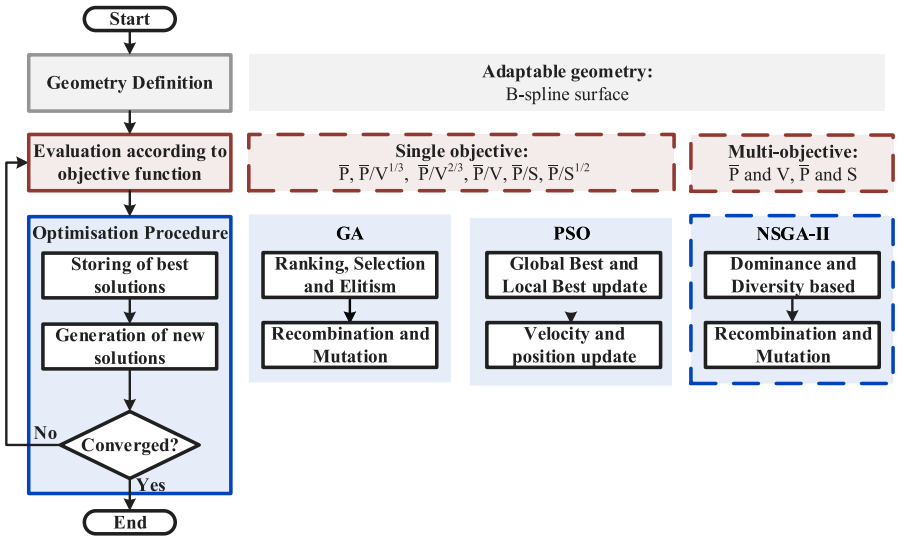

Fig. 1. Flow chart of the optimisation procedure showing an overview of the studied elements. The most suitable objective functions considering combinations of overall mean annual produced power $\bar{P}$, submerged volume V, and submerged surface area S are studied. This is done in single-objective formulations applying Genetic Algorithms (GAs) and Particle Swarm Optimisation (PSO) algorithms. These are compared with a multi-objective optimisation formulation using the NSGA-II algorithm [25].

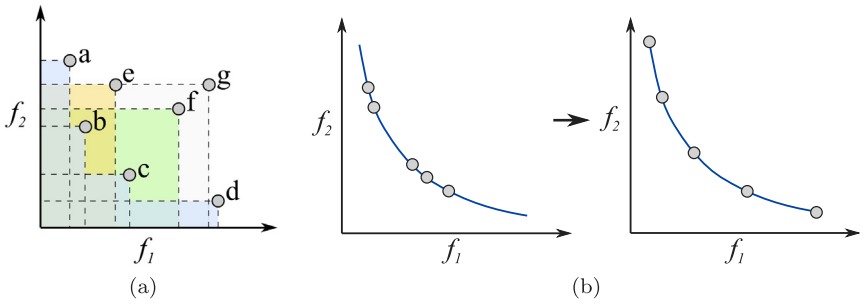

Fig. 2. Schematic representation of bi-objective optimisation solution characteristics: (a) Pareto dominance, (b) Diversity and spread [25].
Source: Adapted from [28].

2. **Diversity**
   The solutions of the estimated Pareto front should be uniformly distributed.
3. **Spread**
   The solutions of the estimated Pareto front should represent the whole spectrum of solutions within the Pareto front. This requires evaluating solutions at the limits of the true Pareto front.

These goals are represented in Fig. 2, where in (b) the concepts of diversity and spread can be visualised.

In the present study, a number of implementations for the multi-objective formulation will be first evaluated, to find the most suitable implementation — as was done for the single-objective algorithms in [26]. The best results from the most suitable multi-objective implementation will then be compared to the best single-objective results by comparing the respective objective function values when using different objective functions.

2.2. Geometry definition

A geometry definition capable of generating very diverse shapes is used, due to its proven ability to generate more optimal results [26]. This approach was first suggested by McCabe in [4] and was extended for its applicability to a wider range of problems in [26]. The WEC hull geometry is defined based on a polyhedron with an x–z-symmetry plane, as shown in Fig. 3. Following the interpolation method that was demonstrated to result in better performing shapes in [30], further points are interpolated between the corner points. They all serve as control points to build a bi-cubic B-spline surface. These vertices can move randomly in space within the defined limits. Some of the vertices' coordinates are fixed, since the vertices lie on the free surface or on the symmetry plane, but the rest (22 in total) can be changed randomly within defined ranges. Note that spherical coordinates (r_n, θ_n, ϕ_n) are used for each vertex v_n.

The 22 coordinates represent the 22 design variables $(x_1, x_2, \ldots, x_{22})$ considered in the optimisation. Upper and lower bounds are defined for these variables to ensure that resulting shapes were closed and not self-crossing:

$$
\begin{aligned}
2.5\ \text{m} \leq r_n &\leq 12.5\ \text{m} && | n = 1, \ldots, 11 \\
-7\pi/16 \leq \theta_n &\leq -\pi/16 && | n = 4, 5, 6, 10, 11 \\
\pi/16 \leq \phi_n &\leq 15\pi/16 && | n = 3, 6 \\
\pi/16 \leq \phi_n &\leq \pi/2 && | n = 2, 5 \\
\pi/2 \leq \phi_n &\leq 15\pi/16 && | n = 8, 10.
\end{aligned}
$$

Additional constraints are applied, that define design variable limits with respect to each other:

$$\phi_2 \leq \phi_3 \leq \phi_8,$$
$$\phi_5 \leq \phi_6 \leq \phi_{10}.$$

Finally, a constraint was defined based on the shape's submerged volume to avoid the optimisation converging on very small or very

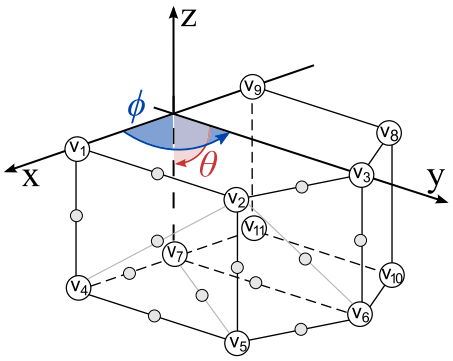

Fig. 3. Geometry definition based on a polyhedron with numbered vertices v_n and vertex coordinates (r_n, θ_n, ϕ_n). Additionally, some example representations of interpolated points are shown in grey [31].
Source: Adapted from Figure 1 in [4].

large shapes. Refer to [26] for further implementation details.

$250\ \text{m}^3 \leq V \leq 4000\ \text{m}^3$

2.3. Geometry evaluation according to objective function

When exploring the best WEC designs, the goal is to find solutions that maximise overall mean power generation and minimise overall costs. To represent power generation the overall mean annual power produced at a given location is used. This is because, as discussed in [9], in cases where proxies for power are used, such as oscillation velocity or RAOs, or calculating mean power absorption for a single sea state, the absorption capabilities of the device are not considered and resulting shapes may not be optimal in real sea conditions. To represent costs, common proxies have been based on the device size measured in terms of submerged volume or submerged surface area. Characteristic lengths and widths have also been used, which are not recommended in [9] since they will strongly depend on the type of device considered and so do not support comparison. For this reason, submerged volume and submerged surface area are considered here to represent costs.

Manufacturability considerations for WEC geometry optimisation were discussed in [32], which highlighted that the presence of high curvatures or double curvatures can increase manufacturing complexity. However, design for manufacturability is not the focus of this study, where a more generic approach for early stage design creation is pursued. So at this stage, to allow for a broader search of the design space free of designer bias, it is assumed that (1) the goal is to generate potentially more suitable shapes without constraining the design process more than necessary, (2) if a certain design shows significant advantages the manufacturing process may be developed later. Since the goal is also to find the most suitable objective function to generate shapes with characteristics that result in reduced costs, the manufacturability aspect is only discussed qualitatively based on the general features of the resulting shapes.

The suitability of the objective function is, therefore, discussed based on two main aspects. Firstly, the difference in achieved values for mean annual produced power, submerged volume and submerged surface area is assessed when applying the different objective functions. Secondly, the resulting shapes are compared qualitatively in terms of their general features and how these are expected to impact on their structural integrity and manufacturability characteristics.

The approaches used to represent overall mean annual power generation and costs are introduced here, whereas the considered case studies, in terms of the investigated objective functions and the approach for their comparison, are introduced in Section 3.1.

Overall mean annual produced power calculation

The overall mean annual power $\bar{P}$ is assessed at a particular location by calculating the mean produced power for a number of sea states taking into account their occurrence probability. Each sea state is defined through a significant wave height H_{m0} and energy period T_e. The wave climate is described using irregular waves represented by a Bretschneider spectrum for a location off the West-Shetland shelf. The corresponding scatter diagram can be found in [4], for which the mean power transported per metre of crest length averaged over a year amounts to 72.8 kW/m. The hydrodynamic behaviour of a shape is analysed using WAMIT [33] a Boundary Element Method based software. WAMIT is a linear radiation/diffraction panel method which solves for the response of floating or submerged bodies moving under the action of surface waves. Frequency-domain methods such as WAMIT (other examples include Nemoh [34] and Ansys Aqwa [35]) have been used extensively to model WECs and WEC arrays. Examples of such studies include [36], where Nemoh and WAMIT results were compared. The power production is then assessed with the help of a pseudo time-domain model. This model is based on a frequency-domain method which uses a semi-optimal impedance matching control, that tunes the WEC to resonate at the energy period (T_e) of each sea state. The oscillation time series $\xi(t)$ is then calculated to be able to apply PTO rating ($P_{PTO,MAX}$) and stroke (ξ_{MAX}) constraints for the power calculation. It should be noted that the PTO characteristics and the chosen control strategy will influence the outcome of the optimisation [37,38], and coupled geometry and PTO optimisation should be considered in the future [18]. Finally, a constraint was applied based on the maximum capture width CW_{MAX} of an axisymmetric body depending on the modes of motion i and the power per metre crest length P_{pm} in deep water conditions in the considered sea state. All the mentioned constraints are defined below.

$$\begin{aligned} \xi_{MAX}(i) &= 5\ \text{m} \quad | \, i = 1,2,3 \\ \xi_{MAX}(i) &= \pi/4 \quad | \, i = 4,5,6 \\ \xi_{MIN}(i) &= -\xi_{MAX}(n) \quad | \, i = 1,2,3,4,5,6 \\ P_{PTO,MAX} &= 2.5\ \text{MW} \\ 0\ \text{MW} \leq \bar{P}(H_{m0}, T_e) &\leq \text{CW}_{MAX} \cdot P_{pm} \end{aligned}$$

In the original implementation a surging only device was considered [4]. The implementation of the hydrodynamic model was, however, expanded to be able to consider devices oscillating in any DoF and combinations of those (see [39]).

To discuss the most suitable approaches for WEC hull geometry optimisation a single DoF and a multiple-DoF case are studied here: a surging only device, and a surging, heaving and pitching device. The behaviour of the optimisation problem is expected to be similar for other single-DoF (e.g. heaving only devices) and multi-DoF cases (e.g. surging and heaving devices), and so the particular cases considered here are chosen to serve as reference cases.

Submerged volume calculation

The software used to calculate the hydrodynamic coefficients for each geometry, WAMIT, also provides their submerged volume calculated with three different approaches. The average of those three values is used as the submerged volume for each shape.

Submerged surface area calculation

Three different ways (Method I, Method II, and Method III) of calculating the geometry's submerged surface area were investigated to find the best trade-off between accuracy and computational time. These were based on the summation of areas of triangular surfaces of a discretised geometry representation and on the integration of the parametric surface description.

Since the geometry is defined through a bi-cubic B-spline surface, some background is given in the supplementary material (Appendix B) on the bi-cubic B-spline surface calculation. In brief, such surface will

be defined as a parametric function $\mathbf{R}(u,v)$ for the parametric directions u and v.

From the parametric integral

The most accurate approach uses the parametric surface function (4) to obtain the surface area. This will therefore be used as the reference approach and will be referred to as 'Method I' and its respective surface area representation as S_I.

$$S_I(u,v) = \int_{u=u_{min}}^{u=u_{max}} \int_{v=v_{min}}^{v=v_{max}} \left|\mathbf{r}_u \times \mathbf{r}_v\right| du\,dv \quad \text{where} \quad \mathbf{r}_u = \frac{\partial \mathbf{R}(u,v)}{\partial u}, \mathbf{r}_v = \frac{\partial \mathbf{R}(u,v)}{\partial v} \tag{4}$$

It should be noted that because $\mathbf{R}(u,v)$ is defined piecewise, the surface area S_I has to be calculated through piecewise integration in intervals of $[u_{min}, u_{max}] = ([u_0,u_1],\dots,[u_{m-1},u_m])$ and $[v_{min}, v_{max}] = ([v_0,v_1],\dots,[v_{n-1},v_n])$.

From a discretised surface

The submerged surface can be discretised into squares by evaluating the surface S represented by $\mathbf{R}(u,v)$ at a discrete number of values of u and v (Method II), or by using the low-order mesh outputted by WAMIT (Method III), which is generated from the bi-cubic B-spline surface description. The low-order panels are obtained by making use of the WAMIT parameter ILOWGDF, which instructs the program to calculate the low-order panels based on the indicated resolution.

In both cases, a number of points representing the surface are available which are not necessarily co-planar. For this reason, calculating the surface area of the quadrilaterals would require a projection of the points onto a common plane. By dividing the surface into triangles instead, this problem is overcome without additional operations. The total surface area is then approximated as the addition of all the triangular surface areas.

Method selection

These three methods were implemented and compared based on accuracy and the required computation time. As mentioned before, Method I is the most accurate method, and is used as the reference case for comparison. The results show that the surface area is slightly overestimated when using Method III and underestimated when using Method II. The lowest calculation time (2s) is achieved with Method III for ILOWGDF=20 (equivalent to approximately 30,000 panels), which also results in only 0.073% difference in surface area from the reference case (Method I). Method III, therefore, shows the best trade-off between computational time and surface area calculation accuracy and was, thus, used within the optimisation algorithm to evaluate the surface area of the generated geometries. This method should be generally applicable for any hull shape modelled in WAMIT.

3. Case studies

3.1. Geometry evaluation according to the objective function

Optimal shapes resulting from optimisation processes where volume was used as a proxy for costs, tend to have complex shapes with increased surface area, despite a reduction in the volume. This can be observed from the initial results presented in [39]. Instead submerged-surface-area-based cost proxies are recommended since these will be representative of the amount of material required for manufacturing and, hence, costs. This agrees with the reasoning followed by Driscoll et al. [40], who proposed representing structural costs through the device surface area and a representative hull thickness for the Wave Energy Prize. The fact that different metrics have been used in the past based on diverse arguments shows the importance of investigating the suitability of different metrics for cost representation in the objective function.

The overall mean annual produced power $\bar{P}$ and the displaced volume V were employed in the objective functions of the original implementation [4], where the volume's cube root was used as a proxy for a characteristic length. The following objective functions were minimised in [4] and are, therefore, again employed here.

$$f_1 = -\bar{P} = f(x_1, x_2, \dots, x_{22}), \tag{5}$$

$$f_2 = -\frac{\bar{P}}{\sqrt[3]{V}} = f(x_1, x_2, \dots, x_{22}), \tag{6}$$

$$f_3 = -\frac{\bar{P}}{V} = f(x_1, x_2, \dots, x_{22}). \tag{7}$$

New objective functions are introduced based on the submerged surface area S, where its square root is also used as a proxy for a characteristic length, and the displaced volume raised to the power of 2/3 is used as a proxy for the submerged surface area. These objective functions are also set to be minimised within the present optimisation process.

$$f_4 = -\frac{\bar{P}}{V^{2/3}} = f(x_1, x_2, \dots, x_{22}), \tag{8}$$

$$f_5 = -\frac{\bar{P}}{S} = f(x_1, x_2, \dots, x_{22}), \tag{9}$$

$$f_6 = -\frac{\bar{P}}{\sqrt{S}} = f(x_1, x_2, \dots, x_{22}). \tag{10}$$

The suitability of the objective function is discussed based on the achieved values for $-\bar{P}$, V and S and the WEC hull geometries obtained when using these different objective functions.

3.2. Optimisation procedure

Both single and multi-objective formulations have been used in the past for WEC hull geometry optimisation. To discuss the suitability of the different formulations and the objective functions used in each case, results from single and multi-objective formulations will be compared. The most suitable algorithm implementations used for single-objective formulations were discussed in [26]. For fairer comparison, a similar study is performed here, where different implementations of a multi-objective algorithm are studied first, before the best results from both formulations are compared. Meta-heuristic algorithms are employed for this purpose, since they are more suitable to solve complex problems with many optimisation variables. They are generally able to find a good enough solution within an acceptable time scale, whereas the computational time required with exact methods increases rapidly with problem complexity [41]. That is, in cases where the objective function has multiple maxima and minima, meta-heuristic algorithms have been proven to perform a more effective search of the solution space and are more likely to find global optima when compared to, for instance, gradient-based methods. They also encourage a broader search of the solution space than direct methods, which is critical when working with so many continuous decision variables. The employed implementations and the approaches for comparison are detailed below.

Elitist non-dominated sorting genetic algorithm (NSGA-II)

The NSGA-II algorithm for multi-objective optimisation is well accepted and has proven to consistently generate good solutions for different types of problems. It simultaneously considers elitism and diversity, and has an improved computational efficiency, with computational effort growing quadratically with population size, as detailed in [42]. The NSGA-II algorithm is applied based on the implementation found in [43]. This implementation uses Simulated Binary Crossover (SBX) and Polynomial Mutation (PM). For comparison, the genetic operators employed in the single-objective implementation of Intermediate Recombination and Breeder Genetic Algorithm Mutation [44] are also applied. The main difference between the genetic operators used within the original NSGA-II versus the ones used in the single-objective implementation [4] is that the former employ a polynomial probability distribution for the crossover and the mutation steps. The NSGA-II genetic operators are explained in more detail in [45,46]. A

Table 1
Summary of NSGA-II setting combinations to improve exploration vs exploitation characteristics.

Implementation	N_{Ind}	η_c	η_m	N_{Parents}
I	22	20	20	NA
II	22	10	20	NA
III	22	20	10	NA
IV	22	NA	NA	20
V	44	NA	NA	40

summary of all the above-mentioned genetic algorithm operations is provided in the supplementary material (Appendix B) based on the information available in Refs. [44–46].

The investigated parameter combinations for the NSGA-II algorithm are summarised in Table 1. For the SBX and PM implementations (I–III), small η_c values result in offspring with higher probability of being more widely spread than for higher η_c values. With this method, near parent solutions are more likely to be chosen than with Intermediate Recombination. The value of η_m determines the order of perturbation $\mathcal{O}(1/\eta_m)$ of the normalised optimisation variable. Higher η_m values will, therefore, result in smaller mutations relative to the optimisation variable's value. NSGA-II implementations IV and V are equivalent to the single-objective implementations in [26] GA-I and GA-IV, respectively. They are mainly characterised by the use of a different number of individuals (N_{Ind}) and of parents selected for crossover (N_{Parents}). NSGA-II implementations will from now on be referred to by the number listed in Table 1, for example NSGAII-I referring to implementation I.

Multi-objective algorithm performance indicators

A large number of performance indicators have been proposed to compare the quality of Pareto front approximations obtained from different multi-objective algorithms. A review of a range of indicators is given by Audet et al. in [47], where indicators are classified into four groups cardinality, convergence, distribution and spread, and convergence and distribution indicators.

Audet et al. [47] identify the hypervolume and hyperarea difference[2] metrics, which are convergence and distribution indicators, to be the most relevant performance indicators. Riquelme et al. [48] confirm that the hypervolume is the most used metric in the optimisation research community.

For this reason, the hypervolume metric is introduced in the following based on [47,49]. The hypervolume (HV) measures how much of the solution space is dominated by the approximated Pareto front, by calculating the size of the objective space that is dominated by these solutions. A high hypervolume measure indicates a good approximation of the true Pareto front. This is represented in Fig. 4, where two sets of solutions A and B are represented through the points in grey. The reference point r_{ref} is represented by the blue point and the hypervolume for each of the solution-sets by the blue area.

The main advantages of this measure are that it captures both the closeness to the true Pareto front and the spread of the solutions, and its mathematical properties. It has been proved that the hypervolume will just achieve its maximum value if and only if the approximated Pareto front contains Pareto optimal points. The main disadvantage is that the results are sensitive to the choice of the reference point. Methods for a consistent reference point choice were, however, introduced in [50]. Depending on the choice of the reference point, extreme points can have a bigger weight than other points. Additionally, the HV is computationally expensive to calculate, with computation time increasing exponentially with the number of objectives. For this reason, approximations with reasonable errors are often used. Monte Carlo

[2] The hyperarea difference is a hypervolume equivalent metric for the direct comparison of the performance of two algorithms.

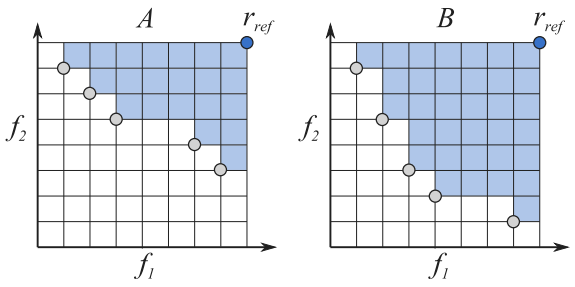

Fig. 4. Representation of the hypervolume measure for two sets of solutions A and B, where $HV(B) > HV(A)$ [25].

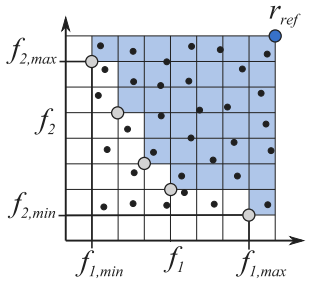

Fig. 5. Representation of the hypervolume measure approximation [25].

sampling [51] of the solution space has been used in multiple approaches, where the hypervolume is used as an objective function and the contribution of each solution to the hypervolume is used as a decision argument to replace solutions in the Pareto front [52,53].

The approximation used here and illustrated in Fig. 5 is based on implementations [54–56]. Random points, shown in black in Fig. 5, are generated within the solution space enclosed within the minimum achieved values of each objective function and the reference point. The reference point, shown in blue in Fig. 5, is defined according to Ishibuchi et al. in [50] for two-objective problems as $r_{ref} = (r, r)$, where $r = 1 + 1/(n_{Sol} + 1)$ with n_{Sol} being the number of solutions in the Pareto front and the solution space being normalised with $r \in [0, 1]$. Then the hypervolume is calculated based on the number of randomly sampled solutions that are dominated by the approximated Pareto front (represented by the grey points in Fig. 5) in relation to the total number of sampled solutions.

Finally, to discuss the suitability of the multi-objective and the single-objective formulations, the best results obtained with the multi-objective optimisation formulation are then compared to the results of the single-objective optimisation formulations, when optimising for $-\bar{P}$ and V simultaneously, as well as when optimising for $-\bar{P}$ and S simultaneously.

4. Results

4.1. Suitability of the objective function

The shapes resulting in the highest overall objective function value from the runs in [26] are used here to analyse the effect of the choice of objective function on the optimal shape. The resulting optimal shapes shown in Figs. A.11, A.12, A.13, A.14, A.15, and A.16 are compared based on their performance, submerged volume and submerged surface area for the surging case in Table 2 and for the surging, heaving and pitching case in Table 3. The corresponding values achieved for $\bar{P}/V$ and $\bar{P}/S$ for all cases can be found in Table 4. Note, for each of the subfigures (a) to (b) in Figs. A.11, A.12, A.13, A.14, A.15, and A.16, there are two images of the corresponding optimal submerged

Table 2
Overview of the optimisation results in terms of the values achieved for $\bar{P}$, V and S for a device oscillating in surge.

Objective Function	Power [kW]	Volume [m^3]	Surface area [m^2]
$f_1 = -\bar{P}$	359.890	3426.843	875.666
$f_2 = -\frac{\bar{P}}{\sqrt[3]{V}}$	240.977	359.994	609.033
$f_3 = -\frac{\bar{P}}{V}$	225.460	255.652	490.557
$f_4 = -\frac{\bar{P}}{V^{2/3}}$	221.750	251.698	456.489
$f_5 = -\frac{\bar{P}}{S}$	200.232	839.501	386.109
$f_6 = -\frac{\bar{P}}{\sqrt{S}}$	345.707	2524.107	781.526

Table 3
Overview of the optimisation results in terms of the values achieved for $\bar{P}$, V and S for a device oscillating in surge, heave and pitch.

Objective Function	Power [kW]	Volume [m^3]	Surface area [m^2]
$f_1 = -\bar{P}$	954.684	2262.850	801.101
$f_2 = -\frac{\bar{P}}{\sqrt[3]{V}}$	775.872	250.209	496.047
$f_3 = -\frac{\bar{P}}{V}$	764.204	250.017	434.857
$f_4 = -\frac{\bar{P}}{V^{2/3}}$	784.169	250.341	460.508
$f_5 = -\frac{\bar{P}}{S}$	505.340	250.071	175.760
$f_6 = -\frac{\bar{P}}{\sqrt{S}}$	677.894	250.336	265.092

geometry. The left image is a view of the geometry from above the free surface and the right image is a view from below the free surface.

Regarding the obtained values for mean annual produced power, submerged volume and submerged surface area shown in Tables 2 and 3, the following can be observed. As expected, the highest value of mean annual power is achieved by geometries optimised to maximise power, which also achieve the highest submerged volume and surface area values. The lowest mean annual power value is achieved by shapes optimised for $f_5 = -\frac{\bar{P}}{S}$. They also achieve, as expected, the lowest surface area value. In the multiple-DoF case, the submerged volume approaches the set lower bound of 250m^3. The volume of optimal shapes resulting from volume-based objective function cost proxies also tend to approach this lower bound.

If comparing the ratios of $\bar{P}/V$ and $\bar{P}/S$ shown in Table 4, it becomes apparent that $f_1 = -\bar{P}$ and $f_6 = -\frac{\bar{P}}{\sqrt{S}}$ result in very similar values in the single-DoF case, which shows that in this case the submerged surface area is not strongly penalised. Additionally, $f_3 = -\frac{\bar{P}}{V}$ and $f_4 = -\frac{\bar{P}}{V^{2/3}}$ show a very similar behaviour. This shows that very little difference in results is obtained from this difference in weighting of the submerged volume in the objective function. Both f_3 and f_4 show lower values for these ratios (around 9 to 32% lower) than $f_2 = -\frac{\bar{P}}{\sqrt[3]{V}}$, apart from the $\bar{P}/V$ ratio in the multi-DoF case where f_3 results in a slightly higher value (1.4% higher than the equivalent f_2-value). This shows that although little difference in the weighting of the submerged volume in the objective function is found between f_3 and f_4, as expected, f_2 does result in a smaller penalisation of the submerged volume in the results.

Regarding the resulting shapes (see Figs. A.11, A.12, A.13, A.14, A.15, and A.16), it becomes apparent that shapes optimised based on volume cost proxies tend to have higher curvatures and thinner cross-sections when compared to shapes optimised based on surface area cost proxies. From a manufacturing and structural integrity perspective, lower curvature, smooth structures of bigger cross-section will have a more even stress distribution. This will also allow for internal structural reinforcement and easier manufacturing, and will, therefore, be more cost efficient. Shapes optimised for power only, tend to have higher volumes, closer to the upper bound of the allowed volume range for the

Table 4
Overview of the optimisation results in terms of the achieved values for $\bar{P}/V$ and $\bar{P}/S$.

Objective Function	Surge		Surge, Heave and Pitch	
	$\frac{\bar{P}}{V}$ [W/m^3]	$\frac{\bar{P}}{S}$ [W/m^2]	$\frac{\bar{P}}{V}$ [W/m^3]	$\frac{\bar{P}}{S}$ [W/m^2]
$f_1 = -\bar{P}$	105.021	410.989	421.894	1191.715
$f_2 = -\frac{\bar{P}}{\sqrt[3]{V}}$	669.392	395.672	3100.901	1564.109
$f_3 = -\frac{\bar{P}}{V}$	881.903	459.601	3056.609	1757.368
$f_4 = -\frac{\bar{P}}{V^{2/3}}$	881.015	485.772	3132.408	1702.836
$f_5 = -\frac{\bar{P}}{S}$	238.513	518.589	2020.783	2875.168
$f_6 = -\frac{\bar{P}}{\sqrt{S}}$	136.962	442.349	2707.938	2557.200

single-DoF case (see Table 2). They also tend to have more spherical shapes. This might be caused by the maximal increase in volume being achieved through a spherical geometry due to limitations in the geometry definition. If comparing the shapes obtained with $f_5 = -\frac{\bar{P}}{S}$ and $f_6 = -\frac{\bar{P}}{\sqrt{S}}$ in the single-DoF case, it can be observed that the shapes are very similar, but scaled-up for f_6, whereas in the multi-DoF case, f_6 generates a shape more similar to the volume-based approaches.

Shapes oscillating in multiple degrees of freedom optimised using a volume-based cost proxy, tend also to result in high surface areas perpendicular to the heave motion (see, for example, Figs. A.13 and A.14). This is due to increases in surface area perpendicular to the heaving motion causing little increase in the displaced volume and resulting in higher objective function values. In the case shown here, the %-contribution of the different modes of motion on power production was: 8% surge, 65% heave, and 15% pitch for $f_3 = -\frac{\bar{P}}{V}$. This is calculated by only considering the diagonal terms of the damping matrix. The remaining percentage stems from the mode-coupling terms. On the other hand, shapes optimised with surface area as a proxy for costs show similar trends with increasing surface areas perpendicular to the direction of oscillation for power extraction, but with a more homogeneous contribution from each of the modes of motion. In the case shown here, the %-contribution of the different modes of motion on power production was: 13% surge, 54% heave, and 46% pitch for $f_5 = -\frac{\bar{P}}{S}$. The sum of these percentages adding up to more than 100 can be explained by the fact that mode-coupling terms can have a negative impact on the total mean annual power.

Due to the used geometry definition, which is more flexible but also more complex, the relationship between surface area and volume becomes looser, when compared, for example, to a sphere, where increases in volume result in increases in surface area and vice versa. At the same time, in terms of hydrodynamics the surface area perpendicular to the mode of motion has a strong influence on the added mass and damping, and the volume on the resonance frequency. When using submerged volume as a proxy for costs, (1) the shape's submerged volume can be reduced significantly without resulting in a significant decrease in submerged surface area and (2) to compensate for the reduced displaced mass, the surface perpendicular to the mode of motion for energy extraction is increased to improve the shapes' hydrodynamic characteristics. This results in shapes optimised using submerged volume as a proxy for costs being more complex and less suitable in practice.

Summary

Overall, regarding the representation of cost in the objective function, shapes resulting from optimisations using submerged surface area as a proxy for costs, result in smoother structures of bigger cross-section and, therefore, easier to manufacture and more adequate from a structural perspective. Regarding the obtained mean annual power, submerged volume and surface area values, $f_5 = -\frac{\bar{P}}{S}$ results in a big decrease in mean annual power values to almost 50% of the mean annual

power achieved by shapes optimised using objective function $f_1 = -\bar{P}$. This would point to a preference for $f_6 = -\frac{\bar{P}}{\sqrt{S}}$ for single-objective optimisation problems. For the multi-DoF case, the shape resulting from optimising for $f_6 = -\frac{\bar{P}}{\sqrt{S}}$ results in a shape with a thin and pointy tail. For this reason, the best trade-off of power maximisation and structural cost reduction among the considered objective functions needs to be investigated further. A multi-objective optimisation study is required to get a better understanding of the resulting optimal shapes for different weightings of the mean annual power and submerged surface area objectives, which is discussed in the following section.

The inclusion of a curvature constraint could be investigated further to avoid sharp edges. Additional considerations that could have an impact on the resulting shapes are viscous effects, particularly for surging devices, and wave directionality effects. Due to the former, more streamlined shapes could be expected. For strongly multi-directional seas, a preference for axisymmetric shapes is foreseeable. The inclusion of these constraints is not expected to have an impact on the preferred objective function. In the case of adding a curvature constraint, an increased convergence difficulty can be expected if applying objective functions using volume-based cost proxies. That is because shapes resulting from the optimisation using this type of objective function tend to display higher curvatures, and so solutions of reduced volume in combination with high curvatures would be disregarded within the optimisation process. If considering surface-area-based cost proxies, this additional constraint would reduce the solution space but a lower impact on the overall optimisation process would be expected. That is because in this case, solutions tend to display shapes of larger cross-section and curvatures, so that less conflict of the curvature constraint with the generated shapes, when using a submerged-surface-area-based cost proxy, is expected. Adding considerations such as viscous effects and wave directionality will likely increase the complexity of the objective function, since it will affect the power calculation, so that the preferred optimisation algorithms might need to be revisited. However, this is not expected to have a significant impact on the choice of the objective function since the power generation vs. cost balance could still be represented through the mean annual power production and the amount of required material based on the submerged surface area.

4.2. Suitability of the optimisation problem formulation

First, the most suitable multi-objective algorithm implementation is investigated by comparing the hypervolume HV of the resulting Pareto fronts. Three runs of each implementation were performed, so that the average HV is employed for fairer comparison. The best Pareto front results obtained from the multi-objective optimisation are then compared to the best results obtained through the single-objective approach applied in [26]. They are compared based on the obtained objective function values and the resulting geometries. The suitability of the optimisation formulation can thus be analysed.

Performance of the multi-objective implementations

For the multi-objective optimisation where mean annual power $\bar{P}$ and submerged volume V were optimised, the performance of the employed algorithms is compared based on the hypervolume measures listed in Tables 5 and 6 for the single-DoF and the multi-DoF cases, respectively. The best resulting Pareto fronts for both cases are represented in Fig. 6. In both cases, it can be observed that the implementations NSGAII-IV and NSGAII-V, using the same recombination and mutation algorithms as in the single-objective cases, achieve the best results. Additionally, an advantage is found in the use of a higher number of individuals in the population, which in NSGAII-V is two times the number of variables. The Pareto front seems to be closer to the true Pareto front, but shows a more reduced spread than achieved with implementations II and III. To understand the effect of each of the objective functions on the optimisation results, extreme solutions should be considered from those implementations, but NSGAII-V was able to find the best $\bar{P}$ and V trade-offs for the practical design range and is selected as the most suitable multi-objective implementation. The runs resulting in the best Pareto fronts (in both cases, Iteration 1 of NSGAII-V) will be used for further analysis.

Table 5
Hypervolume measure (HV) results for multi-objective optimisation with objective functions $-\bar{P}$ and V for cases oscillating in surge only for different NSGA-II implementations. Results for the three optimisation run iterations (It) are shown here.

Implementation	HV			
	It 1	It 2	It 3	Average
I	0.685	0.681	0.667	0.678
II	0.671	0.695	0.695	0.687
III	0.695	0.698	0.702	0.699
IV	0.720	0.721	0.718	0.720
V	0.724	0.717	0.723	0.722

Table 6
Hypervolume measure (HV) results for multi-objective optimisation with objective functions $-\bar{P}$ and V for cases oscillating in surge, heave and pitch for different NSGA-II implementations. Results for the three optimisation run iterations (It) are shown here.

Implementation	HV			
	It 1	It 2	It 3	Average
I	0.534	0.551	0.542	0.542
II	0.533	0.557	0.529	0.540
III	0.568	0.553	0.553	0.558
IV	0.585	0.547	0.575	0.569
V	0.579	0.568	0.578	0.575

Table 7
Hypervolume measure (HV) results for multi-objective optimisation with objective functions $-\bar{P}$ and S for cases oscillating in surge only for different NSGA-II implementations. Results for the three optimisation run iterations (It) are shown here.

Implementation	HV			
	It 1	It 2	It 3	Average
I	0.553	0.553	0.553	0.553
II	0.556	0.551	0.551	0.553
III	0.561	0.555	0.547	0.554
IV	0.557	0.556	0.546	0.553
V	0.565	0.567	0.576	0.569

Table 8
Hypervolume measure (HV) results for multi-objective optimisation with objective functions $-\bar{P}$ and S for cases oscillating in surge, heave and pitch for different NSGA-II implementations. Results for the three optimisation run iterations (It) are shown here.

Implementation	HV			
	It 1	It 2	It 3	Average
I	0.589	0.567	0.594	0.583
II	0.580	0.585	0.594	0.586
III	0.582	0.584	0.582	0.583
IV	0.593	0.594	0.594	0.594
V	0.594	0.594	0.603	0.597

For the multi-objective optimisation where mean annual power $\bar{P}$ and submerged surface area S were optimised, the performance of the employed algorithms is compared based on the hypervolume measures listed in Tables 7 and 8 for the single-DoF and the multi-DoF cases, respectively. The resulting Pareto fronts for both cases are represented in Fig. 7. As in the previous case, implementation NSGAII-V, achieves the best results, both for the single DoF and the multi-DoF cases. The best Pareto front results were obtained in Iteration 1 with NSGAII-IV in the single-DoF case, and in Iteration 1 with NSGAII-V in the multi-DoF case. These results will be used for further analysis.

Overall, Pareto fronts resulting from the optimisation of $-\bar{P}$ and S seem to converge into similar quality solutions, whereas the quality of the Pareto fronts resulting from the optimisation of $-\bar{P}$ and V is more varied. That is, in the case of $-\bar{P}$ and S the Pareto fronts obtained with the five different implementations converge on similar performing

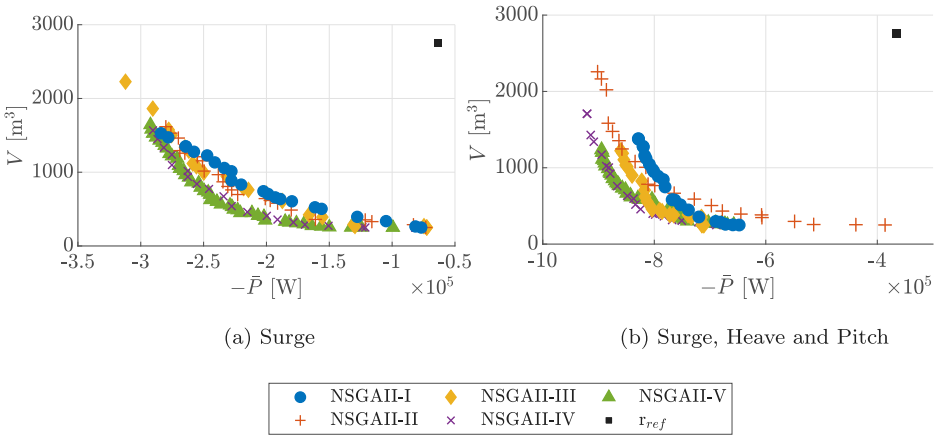

Fig. 6. Pareto fronts for multi-objective optimisation with objective functions $-\bar{P}$ and V [25].

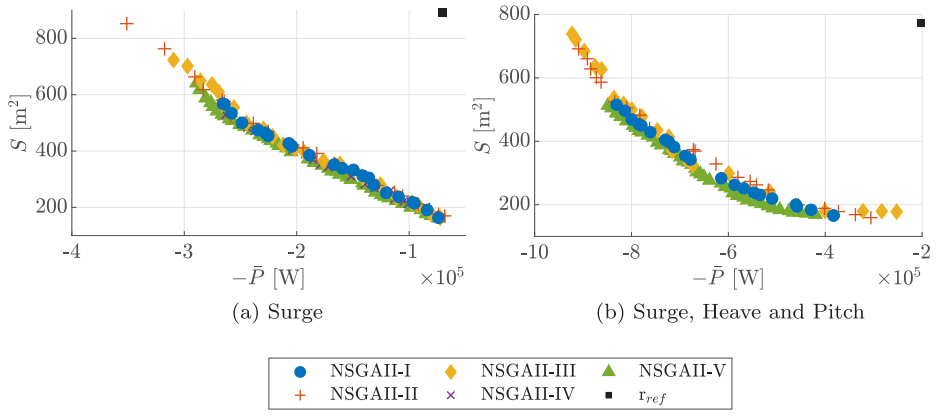

Fig. 7. Pareto fronts for multi-objective optimisation with objective functions $-\bar{P}$ and S [25].

solutions, which is not the case for $-\bar{P}$ and V. This, as in the single-objective cases, could be an indicator of the solution space being more complex for the combination of $\bar{P}$ and V.

Single versus multi-objective optimisation formulation

The results of the single and multi-objective optimisation formulations are represented jointly in the 3-dimensional space, spanned by $\bar{P}$, V and S in Fig. 8 for (a) single and (b) multi-DoF oscillating devices.

In both cases, the single-objective implementations containing mean annual power and submerged volume achieve better solutions in terms of $\bar{P}$ and V than the ones achieved with the multi-objective implementation. That is, shapes resulting from the single-objective implementations achieve higher $\bar{P}$ values for the same V value in comparison to the Pareto front resulting from the multi-objective implementation. Analogously, this is also the case for single-objective implementations containing mean annual power and submerged surface area in terms of the achieved $\bar{P}$ and S values. In the multi-DoF case, it can be seen from the Pareto front that surface area is not strongly affected by the increase in submerged volume and mean annual power in the case optimised for $\bar{P}$ and V. In contrast to this, the Pareto front from the simultaneous optimisation of $\bar{P}$ and S, shows an increase in submerged volume with increasing submerged surface area and mean annual power. On one hand, larger volumes are advantageous to increase the resonance period and with it the annual energy production,[3] however, increases in volume can only be achieved through increases in surface area. For this reason, when using submerged surface area as a proxy for costs an approximately linear increase of submerged volume with submerged surface area can be observed along the Pareto front. On the other hand, when employing submerged volume as a proxy for costs, a point is reached where no advantage is found in increasing submerged surface area with increasing volume. This is because, in this case, the size of the waterplane area determines the power extraction in heave, which in the multi-DoF case has the largest contribution. So when the maximum value for the waterplane surface area has been reached, volume is increased without further significantly increasing the surface area. This can also be observed, to a lesser extent, for the single-DoF case.

In Fig. 9 the resulting shapes at the extremes of the Pareto front and for the median are represented for the surging only case, and in Fig. 10 for the surging, heaving and pitching case. From these figures it can be seen, that the size of the floating body reduces with increasing weight of the cost proxy. In case of the submerged surface area cost proxy, the shape is approximately maintained and the size is reduced, whereas with the submerged volume cost proxy the shape seems to become more slender and complex. This points again to the better suitability of submerged-surface-area-based cost proxies. However, when comparing the results of $f_6 = -\frac{\bar{P}}{\sqrt{S}}$ with respect to the Pareto front, they seem to lie in almost opposite regions of the solution space for the single and the multi-DoF cases.

[3] In the current case, increases in volume result in the resonance period better aligning with the energy periods of the sea states, and that, in turn, results in overall larger power production. Note, however, that for instance a thin cylinder with a large draft has a low natural frequency in heave.

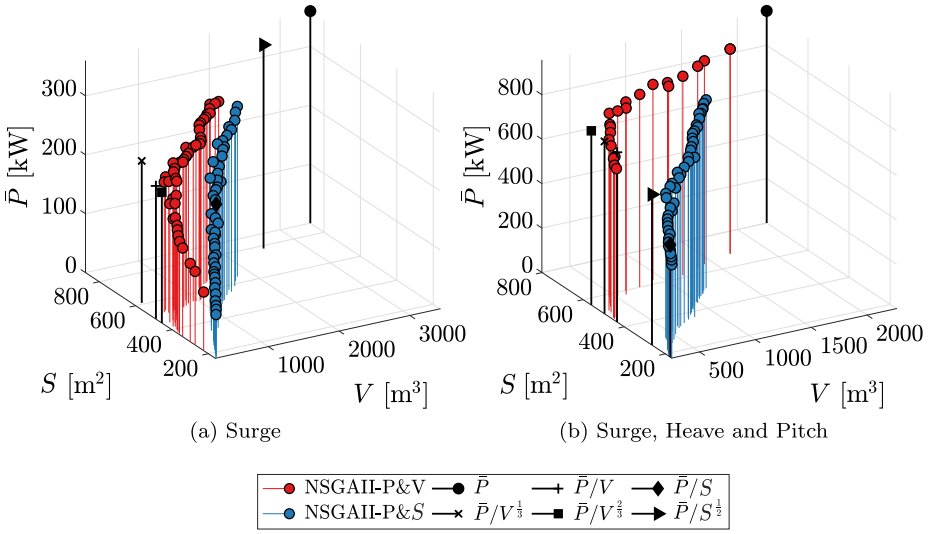

Fig. 8. Pareto fronts from multi-objective optimisation and optimal solutions from single-objective optimisation in 3D-space. The lines are drawn as a visual aid to show mean annual power production [25].

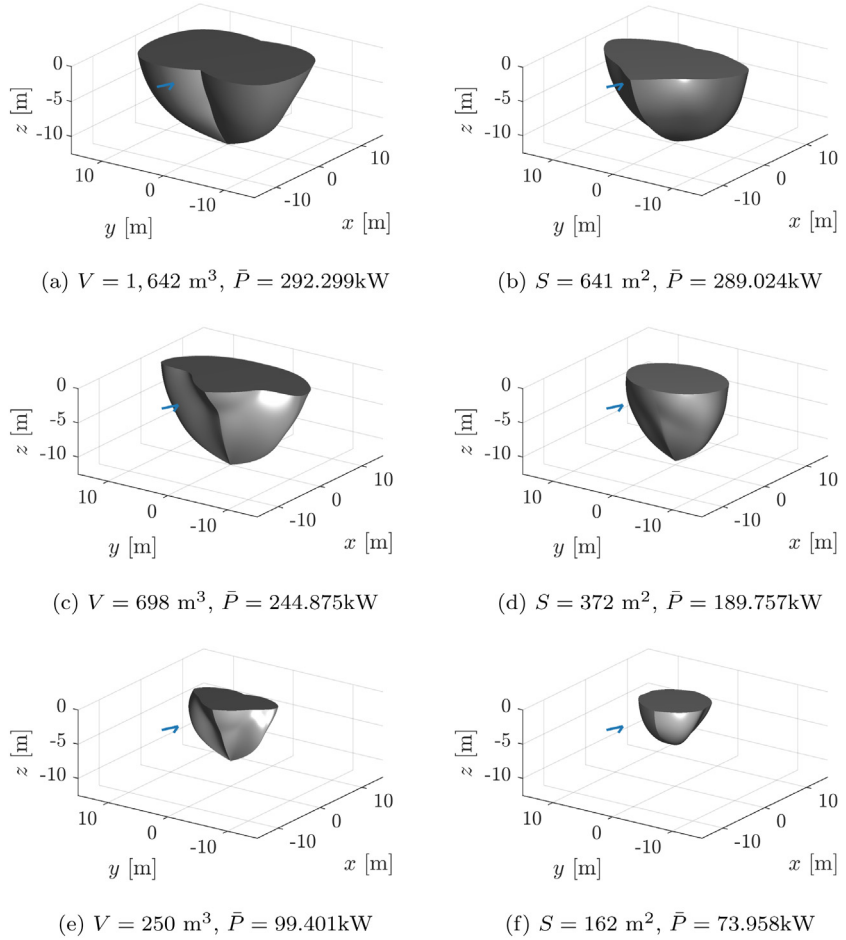

Fig. 9. Optimal shapes for a surging only device on the $\bar{P}$-V-Pareto front (a), (d) and (e), and on the $\bar{P}$-S-Pareto front (b), (d), (f). (a) and (b), and (e) and (f) represent the respective Pareto front limits, and (b) and (c) represent an optimal geometry in the central area of each Pareto front [25].

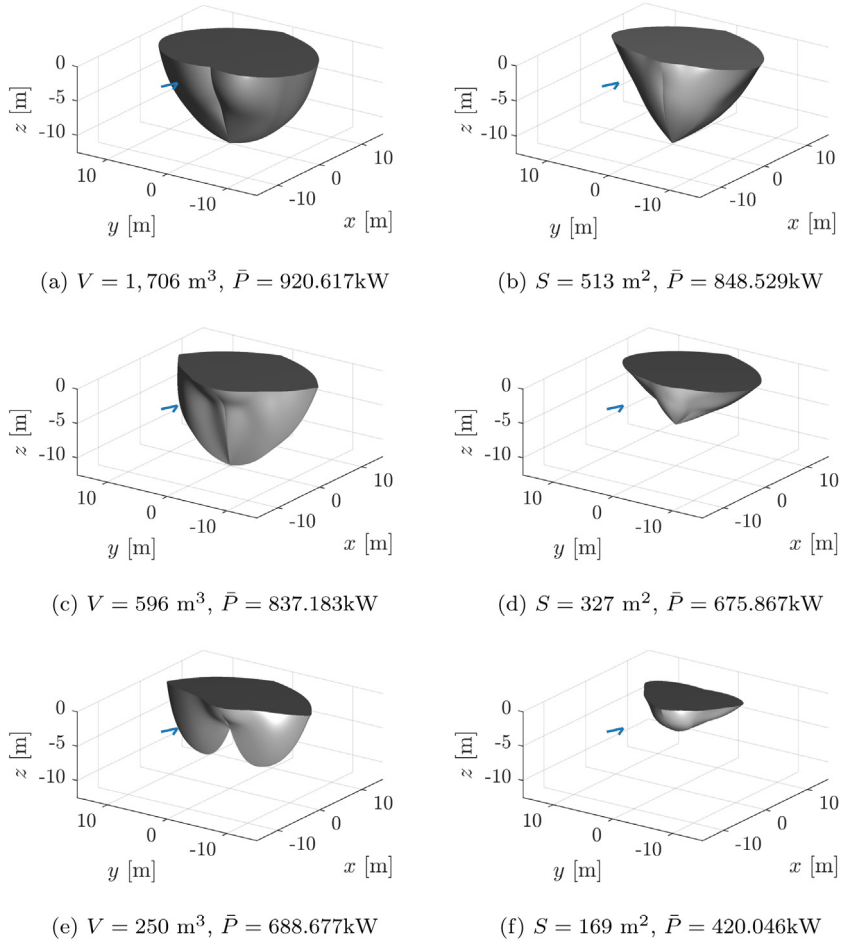

(a) $V = 1,706\ \mathrm{m}^3$, $\bar{P} = 920.617\mathrm{kW}$ (b) $S = 513\ \mathrm{m}^2$, $\bar{P} = 848.529\mathrm{kW}$

(c) $V = 596\ \mathrm{m}^3$, $\bar{P} = 837.183\mathrm{kW}$ (d) $S = 327\ \mathrm{m}^2$, $\bar{P} = 675.867\mathrm{kW}$

(e) $V = 250\ \mathrm{m}^3$, $\bar{P} = 688.677\mathrm{kW}$ (f) $S = 169\ \mathrm{m}^2$, $\bar{P} = 420.046\mathrm{kW}$

Fig. 10. Optimal shapes for a surging, heaving and pitching device on the $\bar{P}$-V-Pareto front (a), (d) and (e), and on the $\bar{P}$-S-Pareto front (b), (d), (f). (a) and (b), and (e) and (f) represent the respective Pareto front limits, and (b) and (c) represent an optimal geometry in the central area of each Pareto front [25].

Summary

NSGA-II implementations using the genetic operators, as in the single-objective implementations, result in more optimal Pareto fronts. Results from single-objective optimisation formulations show a better trade-off of annual energy production, submerged volume and submerged surface area than results from multi-objective optimisation formulations.

Overall, the use of a single-objective formulation is recommended to obtain an initial shape design, and a multi-objective study using surface area and mean annual power as the objective functions is advised for further understanding of other possible solutions within the design space. Due to the better results obtained for the single-objective case, it is recommended also to use this solution as a starting seed for the multi-objective study.

5. Conclusions

In the present study, the suitability of the methods used for geometry optimisation of Wave Energy Converters (WECs) was investigated with a focus on objective function and optimisation formulation selection. Both single-and multi-objective optimisation formulations were used. The suitability of the algorithms used for single-objective optimisation and the geometry definition used to represent the WEC hull were discussed in [26]. A detailed description of the implemented optimisation and hydrodynamic model can also be found there.

The suitability of the objective function for the single-objective optimisation case was investigated here by considering six different options: $f_1 = -\bar{P}$, $f_2 = -\frac{\bar{P}}{\sqrt[3]{V}}$, and $f_3 = -\frac{\bar{P}}{V}$, $f_4 = -\frac{\bar{P}}{V^{2/3}}$, $f_5 = -\frac{\bar{P}}{S}$, and $f_6 = -\frac{\bar{P}}{\sqrt{S}}$. This was done based on the shapes achieving the best objective values for each objective function. The objective function $f_6 = -\frac{\bar{P}}{\sqrt{S}}$ was found to be most suitable due to resulting shapes exhibiting the best trade-off between power maximisation and structural cost reduction. It was found that using the submerged surface area as a proxy for costs, resulted in smooth structures of bigger cross-section and therefore easier to manufacture and more desirable from a structural perspective. In contrast, submerged-volume-based proxies resulted in more complex structures with thinner cross-sections. However, using the other submerged-surface-area-based objective function $f_5 = -\frac{\bar{P}}{S}$ resulted in shapes that generated only 50% of the mean annual power achieved by shapes optimised using the objective function $f_1 = -\bar{P}$. For this reason, f_6 was chosen as the most suitable objective function for single-objective optimisation studies.

The suitability of the employed algorithm for the multi-objective implementations was discussed. Various multi-objective NSGA-II implementations were applied and compared based on the achieved hypervolumes. Three runs of each implementation were performed here, to (1) find the more suitable multi-objective implementation and (2) achieve a fairer comparison to the single-objective optimisation results, where multiple implementations were compared. The NSGA-II implementation using McCabe's recombination and mutation algorithms [4] performed best, and an advantage was found in using double the number of individuals than the number of decision variables.

The results from the single-objective optimisation were then compared to the Pareto fronts obtained from multi-objective formulations. From the comparison of the best single and multi-objective optimisation results, it can be seen that better results were obtained through the single-objective optimisation, and that the results achieved by f_6 were located in very different regions of the solution space with respect to the Pareto front in the single and the multi-DoF cases.

Based on the performed studies and the above discussion, the following design process is recommended: An initial single-objective run, using $f_6 = -\frac{\bar{P}}{\sqrt{S}}$ together with the appropriate optimisation algorithm as defined in [26], and McCabe's or an equivalent adaptable geometry definition should be performed. The result should then be used as the starting seed for a multi-objective study considering mean annual power and submerged surface area, simultaneously, to obtain a better understanding of the solution space. Potentially, also single-objective results using $f_1 = -\bar{P}$ and $f_5 = -\frac{\bar{P}}{S}$ could be used for seeding to ensure a good spread of the Pareto front.

It should be noted that the above recommended approach was obtained using an approximate hydrodynamic model (i.e. a linear, frequency domain radiation/diffraction code). However, it is felt that the recommendations would still apply if a more accurate hydrodynamic solver had been used.

This method can be used by technology developers to generate improved device designs, but it can also serve funding bodies to assess different technologies, since the suitability of the metrics for design comparison has been evaluated.

CRediT authorship contribution statement

Anna Garcia-Teruel: Conceptualization, Methodology, Software, Validation, Investigation, Visualization, Writing - original draft, Funding acquisition. **Bryony DuPont:** Supervision, Writing - review & editing. **David I.M. Forehand:** Conceptualization, Supervision, Writing - review & editing, Funding acquisition.

Declaration of competing interest

The authors declare that they have no known competing financial interests or personal relationships that could have appeared to influence the work reported in this paper.

Acknowledgements

The authors would like to thank the Energy Technology Partnership (ETP) and UKCMER (Engineering and Physical Sciences Research Council (EPSRC), United Kingdom grants EP/I027912/1 and EP/P008682/1) for funding the Ph.D. project [57] within which this work was performed. Additionally, we would like to acknowledge ETP PECRE for their funding support to make this research collaboration possible.

Appendix A. Optimal geometries for different objective functions and modes of oscillation

See Figs. A.11–A.16.

Appendix B. Supplementary data

Supplementary material related to this article can be found online at https://doi.org/10.1016/j.apenergy.2021.117153.

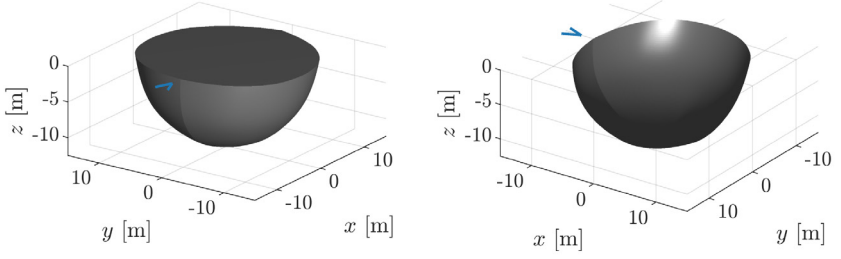

(a) P, Surge

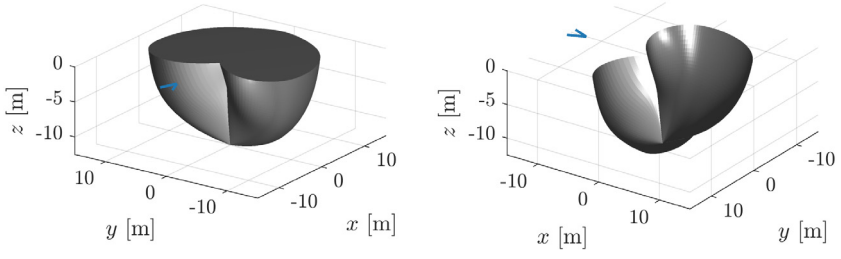

(b) P, Surge, Heave and Pitch

Fig. A.11. Resulting optimal geometries for WECs oscillating in surge only (a) and in surge, heave and pitch (b) optimised for $f_1 = \bar{P}$ [25].

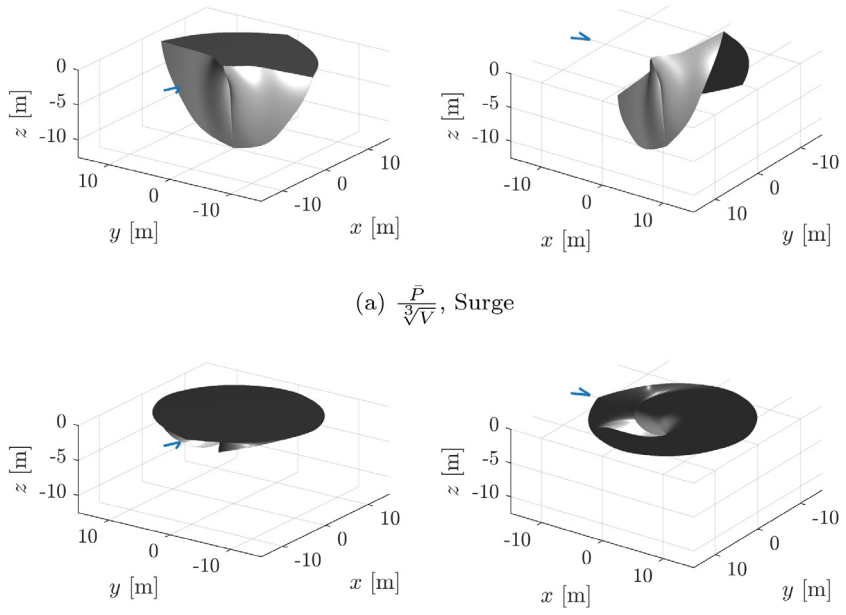

(a) $\frac{\bar{P}}{\sqrt[3]{V}}$, Surge

(b) $\frac{\bar{P}}{\sqrt[3]{V}}$, Surge, Heave and Pitch

Fig. A.12. Resulting optimal geometries for WECs oscillating in surge only (a) and in surge, heave and pitch (b) optimised for $f_2 = \bar{P}/\sqrt[3]{V}$ [25].

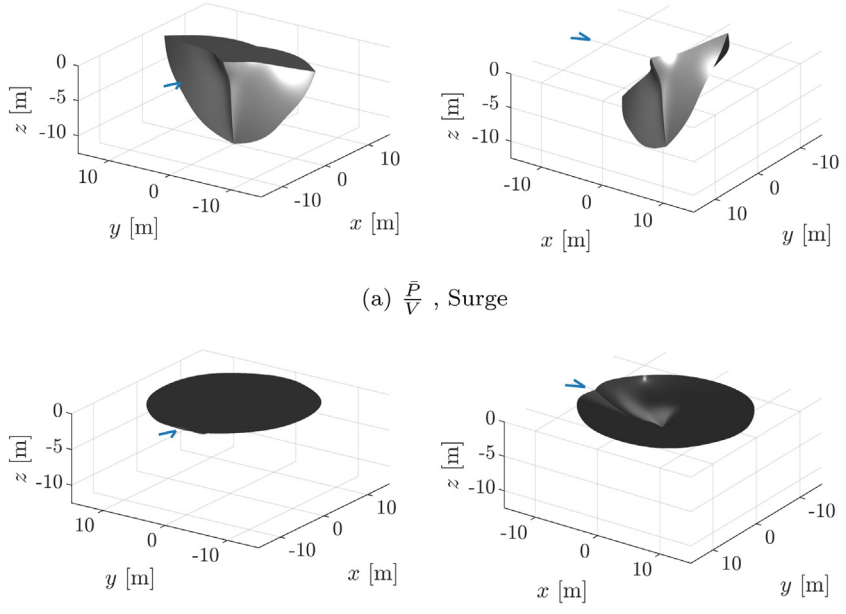

(a) $\frac{\bar{P}}{V}$, Surge

(b) $\frac{\bar{P}}{V}$, Surge, Heave and Pitch

Fig. A.13. Resulting optimal geometries for WECs oscillating in surge only (a) and in surge, heave and pitch (b) optimised for $f_3 = \bar{P}/V$ [25].

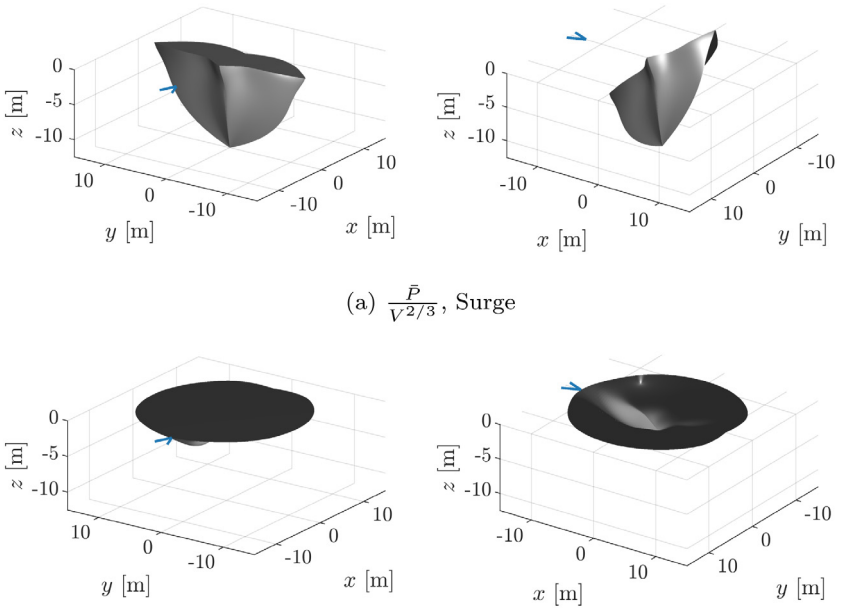

(a) $\frac{\bar{P}}{V^{2/3}}$, Surge

(b) $\frac{\bar{P}}{V^{2/3}}$, Surge, Heave and Pitch

Fig. A.14. Resulting optimal geometries for WECs oscillating in surge only (a) and in surge, heave and pitch (b) optimised for $f_4 = \bar{P}/V^{\frac{2}{3}}$ [25].

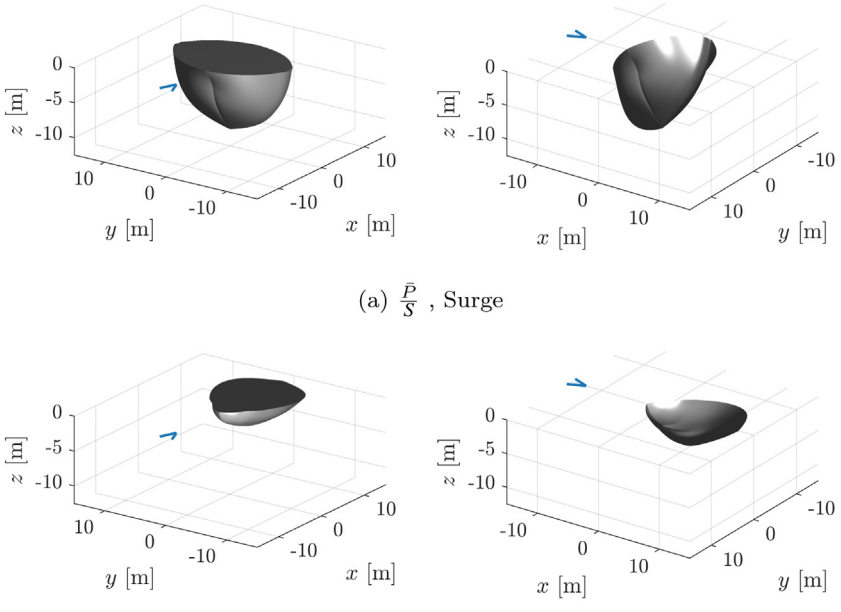

(a) $\frac{\bar{P}}{S}$, Surge

(b) $\frac{\bar{P}}{S}$, Surge, Heave and Pitch

Fig. A.15. Resulting optimal geometries for WECs oscillating in surge only (a) and in surge, heave and pitch (b) optimised for $f_5 = \bar{P}/S$ [25].

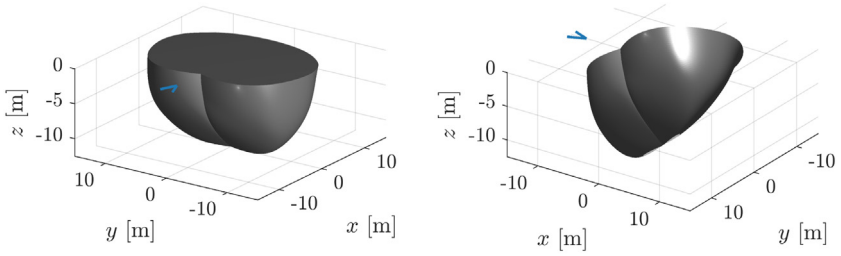

(a) $\frac{\bar{P}}{\sqrt{S}}$, Surge

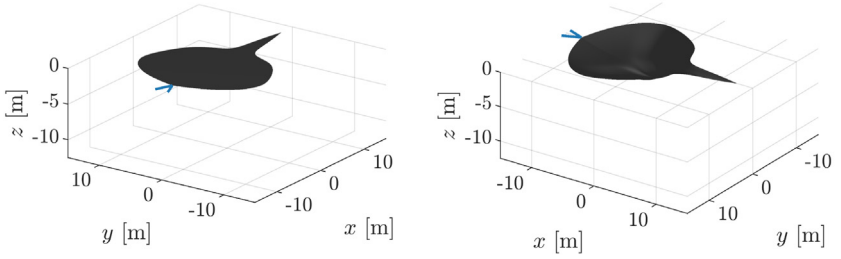

(b) $\frac{\bar{P}}{\sqrt{S}}$, Surge, Heave and Pitch

Fig. A.16. Resulting optimal geometries for WECs oscillating in surge only (a) and in surge, heave and pitch (b) optimised for $f_6 = \bar{P}/\sqrt{S}$ [25].

References

[1] Noel L, Brodie JF, Kempton W, Archer CL, Budischak C. Cost minimization of generation, storage, and new loads, comparing costs with and without externalities. Appl Energy 2017;110–21. http://dx.doi.org/10.1016/j.apenergy.2016.12.060.

[2] Hirvonen J, Kayo G, Hasan A, Sirén K. Zero energy level and economic potential of small-scale building-integrated PV with different heating systems in Nordic conditions. Appl Energy 2016;255–69. http://dx.doi.org/10.1016/j.apenergy.2015.12.037.

[3] Parra D, Zhang X, Bauer C, Patel MK. An integrated techno-economic and life cycle environmental assessment of power-to-gas systems. Appl Energy 2017;440–54. http://dx.doi.org/10.1016/j.apenergy.2017.02.063.

[4] McCabe A. Constrained optimization of the shape of a wave energy collector by genetic algorithm. Renew Energy 2013;51:274–84. http://dx.doi.org/10.1016/j.renene.2012.09.054.

[5] Blanco M, Lafoz M, Ramirez D, Navarro G, Torres J, Garcia-Tabares L. Dimensioning of point absorbers for wave energy conversion by means of differential evolutionary algorithms. IEEE Trans Sustain Energy 2018;1–9. http://dx.doi.org/10.1109/TSTE.2018.2860462.

[6] Kurniawan A, Moan T. Optimal geometries for wave absorbers oscillating about a fixed axis. IEEE J Ocean Eng 2013;38(1):117–30. http://dx.doi.org/10.1109/JOE.2012.2208666.

[7] Costello R, Teillant B, Weber J, Ringwood JV. Techno-economic optimisation for wave energy converters. In: Proc. of the 4h international conference on ocean energy. 2012.

[8] Ribeiro E. Silva S, Gomes RP, Falcaõ AF. Hydrodynamic optimization of the UGEN: Wave energy converter with U-shaped interior oscillating water column. Int J Mar Energy 2016;15:112–26. http://dx.doi.org/10.1016/j.ijome.2016.04.013.

[9] Garcia-Teruel A, Forehand DIM. A review of geometry optimisation of wave energy converters. Renew Sustain Energy Rev 2021;139. http://dx.doi.org/10.1016/j.rser.2020.110593.

[10] Abdelkhalik O, Coe RG, Bacelli G, Wilson DG. WEC geometry optimization with advanced control. In: Proc. of the 36th international conference on ocean, offshore and arctic engineering - volume 10: ocean renewable energy. ASME; 2017, http://dx.doi.org/10.1115/OMAE2017-61917.

[11] Babarit A, Hals J, Muliawan M, Kurniawan A, Moan T, Krokstad J. Numerical benchmarking study of a selection of wave energy converters. Renew Energy 2012;41:44–63. http://dx.doi.org/10.1016/j.renene.2011.10.002.

[12] Weber J, Costello R, Ringwood J. WEC technology performance levels (TPLs)-metric for successful development of economic WEC technology. In: Proc. of 10th European wave and tidal energy conference. EWTEC; 2013.

[13] Jin S, Patton RJ, Guo B. Enhancement of wave energy absorption efficiency via geometry and power take-off damping tuning. Energy 2019;169:819–32. http://dx.doi.org/10.1016/J.ENERGY.2018.12.074.

[14] Shadman M, Estefen SF, Rodriguez CA, Nogueira IC. A geometrical optimization method applied to a heaving point absorber wave energy converter. Renew Energy 2018;115:533–46. http://dx.doi.org/10.1016/J.RENENE.2017.08.055.

[15] Babarit A, Clément AH. Shape optimisation of the SEAREV wave energy converter. In: Proc. of the 9th world renewable energy congress. 2006.

[16] Mavrakos SA, Katsaounis GM, Apostolidis MS. Effect of floaters' geometry on the performance characteristics of tightly moored wave energy converters. In: Proc. of the 28th international conference on ocean, offshore and arctic engineering. Honolulu: ASME; 2009, p. 1145–52. http://dx.doi.org/10.1115/OMAE2009-80133.

[17] Sjökvist L, Krishna R, Rahm M, Castellucci V, Hagnestål A, Leijon M. On the optimization of point absorber buoys. J Mar Sci Eng 2014;2(2):477–92. http://dx.doi.org/10.3390/jmse2020477.

[18] Ringwood JV, Bacelli G, Fusco F. Control, forecasting and optimisation for wave energy conversion. IFAC Proc Vol (IFAC-PapersOnline) 2014;19(2009):7678–89. http://dx.doi.org/10.3182/20140824-6-ZA-1003.00517.

[19] de Andres A, Maillet J, Hals Todalshaug J, Möller P, Bould D, Jeffrey H. Techno-economic related metrics for a wave energy converters feasibility assessment. Sustainability 2016;8(11):1109. http://dx.doi.org/10.3390/su8111109.

[20] Astariz S, Iglesias G. The economics of wave energy: A review. Renew Sustain Energy Rev 2015;45:397–408. http://dx.doi.org/10.1016/j.rser.2015.01.061.

[21] Yu Y-H, Li Y, Hallet K, Hotismky C. Design and analysis for a floating oscillating surge wave energy converter. In: Proc. of 33rd international conference on ocean, offshore and arctic engineering. San Francisco, CA: 2014.

[22] Teillant B, Costello R, Weber J, Ringwood J. Productivity and economic assessment of wave energy projects through operational simulations. Renew Energy 2012;48:220–30. http://dx.doi.org/10.1016/j.renene.2012.05.001.

[23] Garcia-Teruel A, Forehand DIM, Jeffrey H. Metrics for wave energy converter hull geometry optimisation. In: Proc. of the 13th European wave and tidal energy conference. Naples: 2019.

[24] Noad IF, Porter R. Optimisation of arrays of flap-type oscillating wave surge converters. Appl Ocean Res 2015;50:237–53. http://dx.doi.org/10.1016/j.apor.2015.01.020.

[25] Garcia-Teruel A, DuPont B, Forehand DIM. Hull geometry optimisation of wave energy converters: On the choice of the objective functions and the optimisation formulation. figshare, 2021, http://dx.doi.org/10.6084/m9.figshare.14721213.v1.

[26] Garcia-Teruel A, DuPont B, Forehand DIM. Hull geometry optimisation of wave energy converters: On the choice of the optimisation algorithm and the geometry definition. Appl Energy 2020;280. http://dx.doi.org/10.1016/j.apenergy.2020.115952.

[27] Papalambros PY, Wilde DJ. Principles of optimal design: modeling and computation. Cambridge University Press; 2000, p. 416.

[28] Talbi E-G. Metaheuristics: from design to implementation. John Wiley & Sons; 2009, p. 593.

[29] Konak A, Coit DW, Smith AE. Multi-objective optimization using genetic algorithms: A tutorial. Reliab Eng Syst Saf 2006;91(9):992–1007. http://dx.doi.org/10.1016/j.ress.2005.11.018.

[30] McCabe AP, Aggidis GA, Widden MB. Optimizing the shape of a surge-and-pitch wave energy collector using a genetic algorithm. Renew Energy 2010;(12):2767–75. http://dx.doi.org/10.1016/j.renene.2010.04.029.

[31] Garcia-Teruel A, DuPont B, Forehand DIM. Hull geometry optimisation of wave energy converters: On the choice of the optimisation algorithm and the geometry definition. In: Figshare. http://dx.doi.org/10.6084/m9.figshare.13070234.v1.

[32] Garcia-Teruel A, Forehand DIM, Jeffrey H. Wave Energy Converter hull design for manufacturability and reduced LCOE. In: Proc. of the 7th international conference on ocean energy. p. 1–9.

[33] MIT. WAMIT user manual. URL http://www.wamit.com/manualupdate/V70_manual.pdf.

[34] Babarit A, Delhommeau G. Theoretical and numerical aspects of the open source BEM solver NEMOH. In: Proc. of the 11th European wave and tidal energy conference. Nantes, France: 2015.

[35] ANSYS Inc. Ansys aqwa: Hydrodynamics Simulation & diffraction analysis | ansys. URL https://www.ansys.com/products/structures/ansys-aqwa.

[36] Penalba M, Kelly T, Ringwood J. Using NEMOH for modelling wave energy converters: A comparative study with WAMIT. In: 12th European wave and tidal energy conference. Cork: 2017.

[37] Garcia-Rosa PB, Ringwood JV. On the sensitivity of optimal wave energy device geometry to the energy maximizing control system. IEEE Trans Sustain Energy 2016;7(1):419–26. http://dx.doi.org/10.1109/TSTE.2015.2423551.

[38] Bubbar K, Buckham B, Wild P. A method for comparing wave energy converter conceptual designs based on potential power capture. Renew Energy 2018;115:797–807. http://dx.doi.org/10.1016/j.renene.2017.09.005.

[39] Garcia-Teruel A, Forehand DIM. Optimal wave energy converter geometry for different modes of motion. In: Advances in renewable energies offshore: proceedings of the 3rd international conference on renewable energies offshore. Lisbon: 2018. p. 299–305.

[40] Driscoll F, Weber J, Jenne S, Thresher R, Fingersh LJ, Bull D, et al. Methodology to calculate the ACE and HPQ metrics used in the wave energy prize (March 2018). 2018.

[41] Blum C, Roli A. Metaheuristics in combinatorial optimization. ACM Comput Surv 2003;35(3):268–308. http://dx.doi.org/10.1145/937503.937505, URL http://portal.acm.org/citation.cfm?doid=937503.937505.

[42] Deb K, Agrawal S, Pratap A, Meyarivan T. A fast elitist non-dominated sorting genetic algorithm for multi-objective optimization: NSGA-II. In: Proc. of the 6th international conference on parallel problem solving from nature. Springer-Verlag London; 2000.

[43] Baskar S, Tamilselvi S, Varshini P. MATLAB code for constrained NSGA II - file exchange - MATLAB central. File Exchange - MATLAB Central.

[44] Mühlenbein H, Schlierkamp-Voosen D. Predictive models for the breeder genetic algorithm. Evol Comput 1993;1(1):25–49. http://dx.doi.org/10.1162/evco.1993.1.1.25.

[45] Deb K, Kalyanmoy D. Multi-Objective Optimization using Evolutionary Algorithms. John Wiley & Sons; 2001, p. 497, URL http://dl.acm.org/citation.cfm?id=559152.

[46] Deb K, Pratab S, Agarwal S, Meyarivan T. A fast and elitist multiobjective genetic algorithm: NGSA-II. IEEE Trans Evol Comput 2002;6(2):182–97. http://dx.doi.org/10.1109/4235.996017.

[47] Audet C, Cartier SLD, Cartier D, Bigeon J, Salomon L. Performance indicators in multiobjective optimization. Tech. rep., Groupe d'études et de recherche en analyse des décisions; 2018, URL https://www.gerad.ca/fr/papers/G-2018-90.

[48] Riquelme N, Von Lucken C, Baran B. Performance metrics in multi-objective optimization. In: Proc. of the 2015 Latin American computing conference. IEEE; 2015, p. 1–11. http://dx.doi.org/10.1109/CLEI.2015.7360024.

[49] Cheng S, Shi Y, Qin Q. On the performance metrics of multiobjective optimization. In: Tan Y, Shi Y, Ji Z, editors. Advances in swarm intelligence. Berlin, Heidelberg: Springer Berlin Heidelberg; 2012, p. 504–12.

[50] Ishibuchi H, Imada R, Setoguchi Y, Nojima Y. Reference point specification in hypervolume calculation for fair comparison and efficient search. In: Proc. of the genetic and evolutionary computation conference on. New York, USA: ACM Press; 2017, p. 585–92. http://dx.doi.org/10.1145/3071178.3071264.

[51] Lemieux C. Monte Carlo and Quasi-Monte Carlo sampling. Springer series in statistics. New York, NY: Springer New York; http://dx.doi.org/10.1007/978-0-387-78165-5.

[52] Bader J, Deb K, Zitzler E. Faster hypervolume-based search using monte carlo sampling. Berlin, Heidelberg: Springer; 2010, p. 313–26. http://dx.doi.org/10.1007/978-3-642-04045-0_27.

[53] Bader J, Zitzler E. HypE: An algorithm for fast hypervolume-based many-objective optimization. Evol Comput 2011;19(1):45–76. http://dx.doi.org/10.1162/EVCO_a_00009.

[54] Simone. Hypervolume approximation - file exchange - MATLAB central. 2015, URL https://uk.mathworks.com/matlabcentral/fileexchange/50517-hypervolume-approximation.

[55] Cao Y. Hypervolume indicator - file exchange - MATLAB central. 2008, URL https://uk.mathworks.com/matlabcentral/fileexchange/19651-hypervolume-indicator.

[56] Johannes. Hypervolume computation - file exchange - MATLAB central. 2011, URL https://uk.mathworks.com/matlabcentral/fileexchange/30785-hypervolume-computation.

[57] Garcia-Teruel A. Geometry Optimisation of Wave Energy Converters. Doctoral thesis, The University of Edinburgh; 2020.